Direct observation of how the heavy-fermion state develops in $CeCoIn_5$

Q. Y. Chen,[1,2] D. F. Xu,[1] X. H. Niu,[1] J. Jiang,[1] R. Peng,[1] H. C. Xu,[1] C. H. P. Wen,[1] Z. F. Ding,[1] K. Huang,[1] L. Shu,[1] Y. J. Zhang,[3,4] H. Lee,[3] V. N. Strocov,[5] M. Shi,[5] F. Bisti,[5] T. Schmitt,[5] Y. B. Huang,[6] P. Dudin,[7] X. C. Lai,[2] S. Kirchner,[3,8,*] H. Q. Yuan,[3,4,9] and D. L. Feng[1,9,†]

[1]*State Key Laboratory of Surface Physics and Department of Physics, Fudan University, Shanghai 200433, China*
[2]*Science and Technology on Surface Physics and Chemistry Laboratory, Mianyang 621908, China*
[3]*Center for Correlated Matter, Zhejiang University, Hangzhou, 310058, China*
[4]*Department of Physics, Zhejiang University, Hangzhou, 310027, China*
[5]*Swiss Light Source, Paul Scherrer Institute, CH-5232 Villigen PSI, Switzerland*
[6]*Shanghai Institute of Applied Physics, CAS, Shanghai, 201204, China*
[7]*Diamond Light Source, Harwell Science and Innovation Campus, Didcot OX11 0DE, United Kingdom*
[8]*Department of Physics and Astronomy, Rice University, Houston, Texas, 77005, USA*
[9]*Collaborative Innovation Center of Advanced Microstructures, Nanjing 210093, China*

(Received 22 February 2017; revised manuscript received 16 May 2017; published 7 July 2017)

Heavy-fermion systems share some of the strange metal phenomenology seen in other unconventional superconductors, providing a unique opportunity to set strange metals in a broader context. Central to understanding heavy-fermion systems is the interplay of localization and itinerancy. These materials acquire high electronic masses and a concomitant Fermi volume increase as the f electrons delocalize at low temperatures. However, despite the wide-spread acceptance of this view, a direct microscopic verification has been lacking. Here we report high-resolution angle-resolved photoemission measurements on $CeCoIn_5$, a prototypical heavy-fermion compound, which spectroscopically resolve the development of band hybridization and the Fermi surface expansion over a wide temperature region. Unexpectedly, the localized-to-itinerant transition occurs at surprisingly high temperatures, yet f electrons are still largely localized even at the lowest temperature. These findings point to an unanticipated role played by crystal-field excitations in the strange metal behavior of $CeCoIn_5$. Our results offer a comprehensive experimental picture of the heavy-fermion formation, setting the stage for understanding the emergent properties, including unconventional superconductivity, in this and related materials.

DOI: 10.1103/PhysRevB.96.045107

I. INTRODUCTION

Understanding the emergence of superconductivity in exotic metals has remained a challenge ever since the discovery of unconventional superconductivity in the cuprates. Consensus exists that the key to unlocking its physics lies in unraveling the microscopics of the strange-metal phase with its unusual properties [1,2]. Many of the underlying issues as, e.g., proximity to a magnetic instability, quantum criticality, and dynamic scaling behavior have been explored in other materials classes, most notably the heavy fermions whose comparatively high tunability makes them attractive test beds of emergence in strongly correlated electron systems [3]. This tunability in the heavy electron compounds is in part due to the dynamic generation of low-energy scales and the enhancement of the density of states at the Fermi energy (E_F).

Central to understanding heavy-fermion systems is the interplay of localization and itinerancy. According to the standard model of heavy-fermion behavior, the Kondo lattice model [4], f electrons are localized at high temperature (T), while their exchange coupling to conduction electrons leads to the formation of bands with heavy masses as T is lowered and the f electrons become itinerant [5]. This localized-to-itinerant transition is accompanied by a Fermi volume increase, which, for a Kondo lattice model, is expected to equal one electron per unit cell due to the inclusion of the f electrons [6,7]. However, the experimental picture has been puzzling, if not unclear, and direct validation is still lacking [8–10]. An increasing number of heavy-fermion compounds is known to be located in proximity to a magnetic instability and can be tuned through a quantum critical point (QCP). Dynamic or energy-over-temperature (E/T) scaling, and a drastic change in the charge carrier concentration occur near certain QCPs in close analogy of what has been seen in the cuprates [2,11–13]. A complete microscopic picture, however, has so far not emerged as microscopic probes of the electronic state as angle-resolved photoemission spectroscopy (ARPES) and scanning tunneling microscopy (STM) seem to yield inconsistent results [14–16]. A recent ARPES study on $YbRh_2Si_2$ between 95 and 1 K, for example, challenged the picture of a localized-to-itinerant transition, as T is lowered, reporting a T-independent Fermi surface [9] (see, however, Ref. [17]). In contrast, an earlier bulk-sensitive laser-ARPES study of the same compound obtained ≈50 K as the onset temperature for quasiparticle peak formation [8]. For $CeCoIn_5$ on the other hand, a recent STM study reported quantum critical scaling to persist up to a surprisingly high temperature $T \approx 60$ K [15]. Here, we address the formation of the heavy-fermion state, the Fermi volume increase, E/T-scaling and the overall validity of the Kondo lattice model for the prototypical heavy-fermion system $CeCoIn_5$ using state-of-the-art ARPES.

*stefan.kirchner@correlated-matter.com
†dlfeng@fudan.edu.cn

$CeCoIn_5$, a well-studied compound whose low-energy behavior mimics that of the underdoped cuprates, becomes superconducting at a comparatively large $T_c \sim 2.3$ K and displays strange metal behavior above T_c. De Haas-van Alphen (dHvA) [18,19], optical conductivity [20,21], and STM [15,22,23] measurements compare well with band calculations that assume fully itinerant f electrons [18,24], but they are limited by temperature range and the lack of momentum resolution. Peculiar ARPES results [25–27] have been obtained for $CeCoIn_5$: some suggest the Ce $4f$ electrons are itinerant up to 105 K [26], while subsequent results suggest they are predominantly localized at 25 K [27]. A recent review by Fujimori *et al.* stated that f electrons in $CeCoIn_5$ are nearly localized, but finite and partial hybridizations manifest their itinerant properties [14]. The appearance of various T scales in different measurements further complicates the problem. For example, with decreasing T, the resistivity of $CeCoIn_5$ first increases and then decreases just below 50 K [28]. This characteristic T of maximal resistivity, the coherence temperature $T_{\rm coh} \approx 50K$, has been associated with the onset of a coherent heavy electron band, and assumed to be close to the Kondo temperature, T_K. Meanwhile, STM investigations found a scaling of the local conductance in $CeCoIn_5$ below 60 K, which was interpreted in terms of quantum critical E/T scaling [15]. Intriguingly, however, both the Seebeck and the Nernst coefficients of $CeCoIn_5$ exhibit anomalies at around 20 K [29]. The heavy-fermion formation, its characteristic scales, and its interplay with other similar energy scale besides T_K, e.g., crystal-field excitations, have thus remained a matter of debate.

Here, we address these perplexing findings in the prototypical heavy-fermion system $CeCoIn_5$. We combine bulk-sensitive soft x-ray ARPES to unravel its three-dimensional (3D) electronic structure, and resonant ARPES to expose the f-electron behavior in an extended T range with much improved energy resolution. As a result, a comprehensive experimental picture of heavy-fermion formation unfolds with unprecedented precision and details. More importantly, we are able to link the appearance of the heavy-fermion state at higher T to crystal-field physics. Our data show that the size of the Fermi surface is smaller than predicted in DMFT calculations, and gives an explicit and quantitative picture on the degree of localization for the f electrons in $CeCoIn_5$.

Single crystals of $CeCoIn_5$ were grown by an In self-flux method. Room-temperature powder x-ray diffraction measurements revealed that all the crystals are single-phase and crystallize in the tetragonal $HoCoGa_5$ structure. The samples were then cleaved along the c axis in ultrahigh vacuum before performing ARPES measurements. Soft x-ray ARPES data

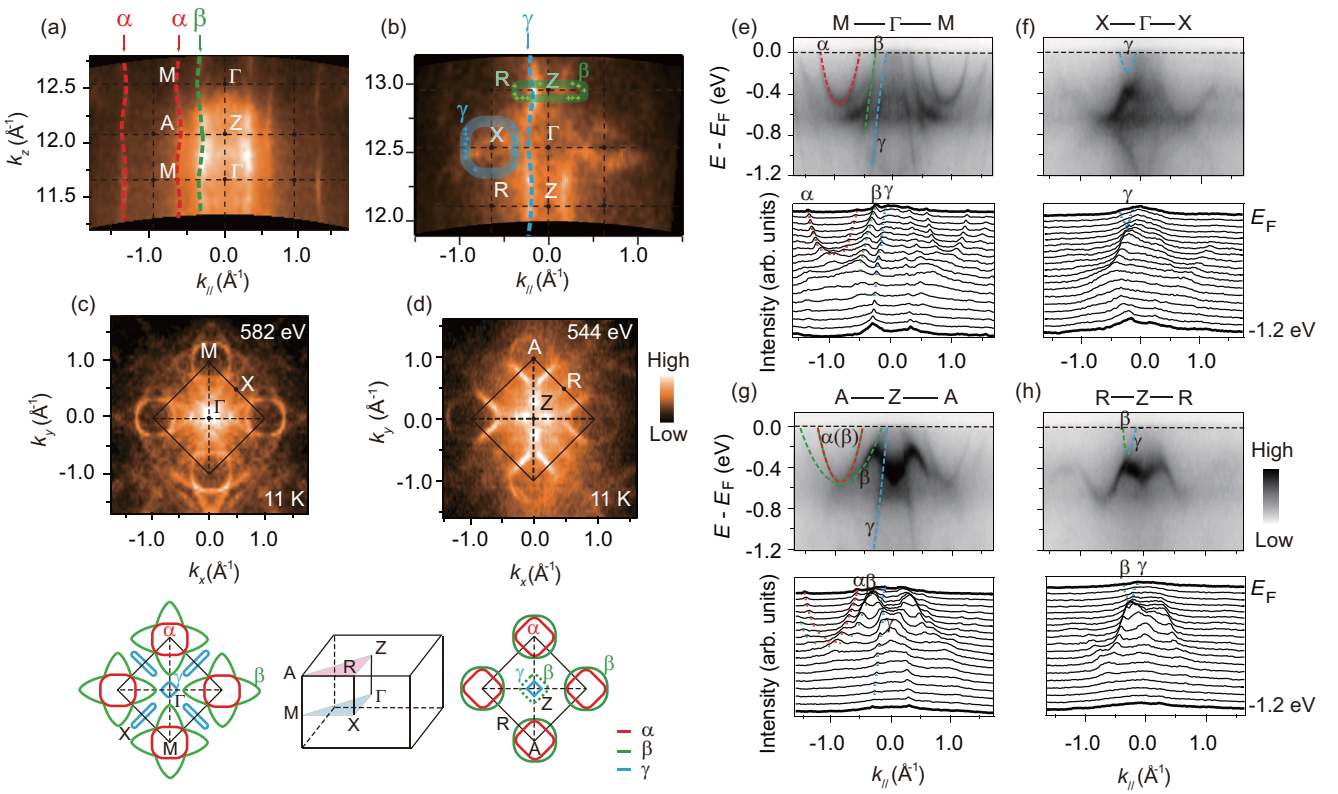

FIG. 1. Three-dimensional electronic structure of $CeCoIn_5$ at 11 K. (a) and (b) Photoemission intensity maps in the ΓZAM plane in (a) and ΓZRX plane in (b), respectively. Different k_zs were accessed by varying the photon energy between 480 and 648 eV. (c) and (d) Photoemission intensity maps in the ΓXM plane in panel (c) and ZAR plane in panel (d) taken with 582 and 544 eV photons, respectively, which were determined based on the periodicity of the high symmetry planes. The inner potential was estimated as 16 eV. The lower panels plot the Fermi surface sheets in the upper panels by tracking Fermi crossings. Part of the β Fermi surface is hard to trace (dashed lines). The Brillouin zone of $CeCoIn_5$ is depicted in the middle. (e)–(h), Photoemission intensity distributions along Γ-M in (e) and Γ-X in (f), Z-A in (g), and Z-R in (h), respectively. Lower panels are their corresponding momentum distribution curves (MDCs). All photoemission intensity data here were integrated over a window of ($E_F - 20$ meV, $E_F + 20$ meV).

shown in Fig. 1 were taken at the Advanced Resonant Spectroscopies (ADRESS) beamline at the Swiss Light Source, with a variable photon energy and PHOIBOS-150 analyzer. The overall energy resolution was 70–80 meV, and the angular resolution was 0.07°. The samples were cleaved and measured at 11 K under a vacuum better than 5×10^{-11} mbar. All the data taken with the on-resonance 121 eV photons [except those in Figs. 4(b) and 4(c)] were obtained at the "Dreamline" beamline of the Shanghai Synchrotron Radiation Facility (SSRF) with a Scienta D80 analyzer. Both *s*- and *p*-polarized photons were used. The polarization of the *p*-polarized light is parallel to the plane defined by the incident light and emitted electrons, while the polarization of the *s*-polarized light is perpendicular to this plane. The samples were cleaved *in situ* at 17 K. The vacuum was better than 5×10^{-11} mbar at 17 K. The energy resolution was 17 meV, and the angular resolution was 0.2°. The data in Figs. 4(b) and 4(c) were taken at Beamline I05-ARPES of the Diamond Light Source, equipped with a Scienta R4000 analyzer. The typical angular resolution was 0.2° and the overall energy resolution was better than 16 meV. The vacuum was kept below 9×10^{-11} mbar. The samples were cleaved at 170 K before performing ARPES experiments.

II. 3D FERMI SURFACE AND BAND STRUCTURE

We start by measuring the 3D electronic structure of $CeCoIn_5$ at 11 K with soft x-ray ARPES, whose bulk sensitivity and high out-of-plane momentum (k_z) resolution make it an effective tool for studying more-3D rare-earth compounds [30]. Although three types of surfaces have been found on the cleavage plane by STM [15], we only detected one set of bands, indicating that the bulk bands dominate the data. Photoemission intensity maps in the ΓZAM plane and ΓZRX plane of the $CeCoIn_5$ Brillouin zone are shown in Figs. 1(a) and 1(b), respectively.

The Fermi surface in the ΓXM plane, shown in Fig. 1(c), is composed of two electron pockets—a flower-shaped β and a rounded α pocket—and two hole pockets—a squarelike pocket around Γ and a narrow racetrack-shaped pocket around X, both attributed to the γ band [Fig. 1(f)]. As shown by the photoemission intensity plot along the Γ-M direction in Fig. 1 e, the α band is parabolic-like with its bottom 0.45 eV below E_F. In the ZAR plane [Fig. 1(d)], the β pocket becomes rounded and the α pocket squarelike. As shown in Fig. 1(g), the β band contributes two Fermi crossings along Z-A, one degenerates with the α band while the other contributes part of the squarelike Fermi surface around Z.

Our data show that the α band is the most two-dimensional (2D). Although the cross-sections of the α and β Fermi surfaces show weak variation in the ΓZAM plane [Fig. 1(a)], obvious differences can be observed between the Fermi surface topologies in the ΓXM and ZAR planes. In the ΓZRX cross-section [Fig. 1(b)], there is a small β-derived pocket around Z and another pocket around X contributed by the γ band, indicating rather 3D characters of these two bands. The shapes of the α and β pockets qualitatively agree with previous dHvA measurements and calculations [18,19]. While dHvA provided little information on the γ band, we find that it contributes a squarelike pocket around Z in the ZAR plane, contradicting the calculation which predicts that the γ Fermi surface does not cross the ZAR plane [18]. The difference may arise from the only partially itinerant f electrons, as will be shown later in this paper. The observed quasi-2D electronic structure is consistent with the moderate in-plane versus out-of-plane anisotropies in the superconducting critical field and magnetic susceptibility [18,28,31].

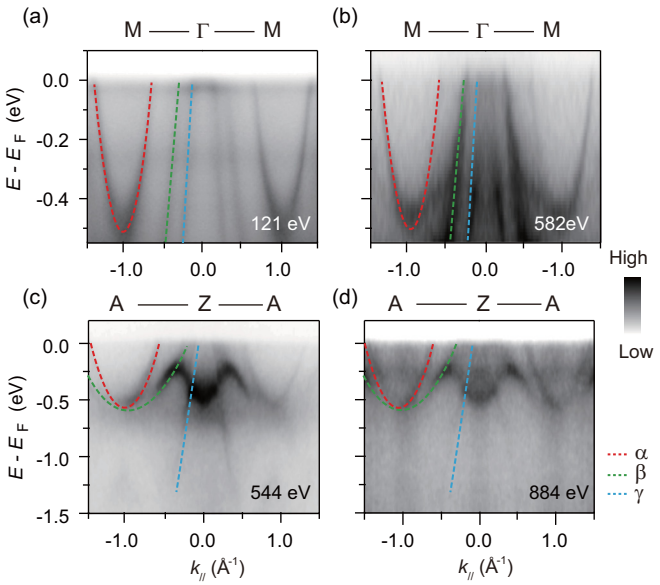

FIG. 2. Comparison of the photoemission intensity distributions taken at various photon energies. (a) and (b) Photoemission intensity distributions along Γ-M taken with (a) 121 and (b) 582 eV, respectively. (c) and (d) Photoemission intensity distributions along Z-A taken with (c) 544 and (d) 884 eV, respectively. The dashed curves indicate the band dispersions.

III. ON- AND OFF- RESONANCE ARPES DATA

Because the f-electron states are not pronounced in the soft x-ray data, we further performed on-resonant ARPES measurements on $CeCoIn_5$ at the Ce $4d$-$4f$ transition (121 eV) to enhance the f electron photoemission matrix element [Fig. 2(a)]. We hereby first prove that 121 eV photons probe the bulk electronic structure of $CeCoIn_5$ in the close vicinity of Γ-M. To show this, we present the photoemission intensity distributions along Γ-M taken with 582 eV photons in Fig. 2(b). The dispersion of the three conduction bands (dashed curves) are almost identical in both cases, while the f electron character is enhanced by the on-resonance excitation in Fig. 2(a). Furthermore, Figs. 2(c) and 2(d) display the photoemission intensity distributions along Z-A taken with 544 and 844 eV, respectively. It is obvious that the spectra taken with 544 and 844 eV are essentially the same. Because the probing depth of 884 eV soft x-ray is about 25 Å according to the universal curve, it is bulk sensitive. Consequently, the photoemission data taken with 544-eV photons is also bulk sensitive, and so are the 582-eV photons. Following the same logic, the fact that the data taken with 582- and 121-eV photons are similar prove that the bulk electronic structure of $CeCoIn_5$ is detected by 121-eV photons. Consistently, because the bulk sensitivity gives high k_z resolution, the fast-dispersing bands in Fig. 2(a) are sharp. The bulk nature of the observed $4f$

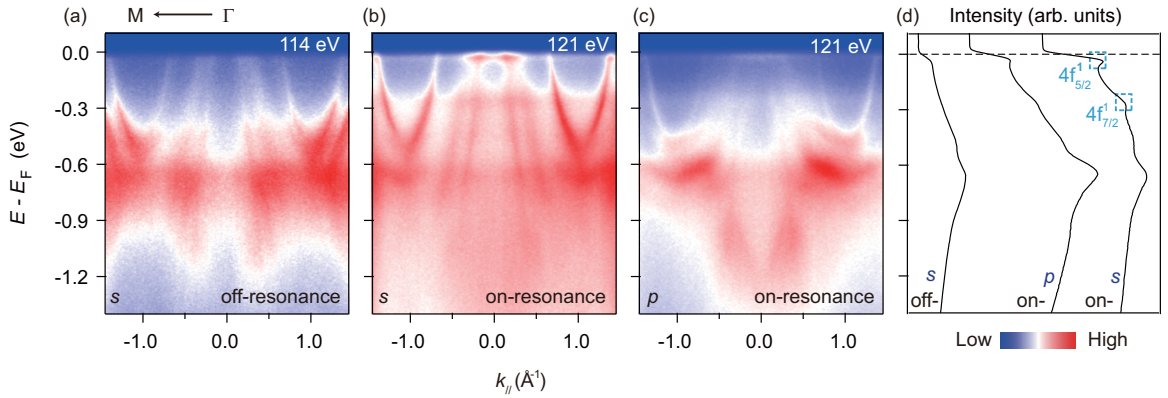

FIG. 3. On-resonance and off-resonance ARPES data of $CeCoIn_5$ at 11 K. (a) and (b) Photoemission intensity distributions of $CeCoIn_5$ taken along Γ-M with off-resonance [114 eV, panel (a)] and on-resonance [121 eV, panel (b)] s-polarized light, respectively. (c) Photoemission intensity distributions of $CeCoIn_5$ taken along Γ-M with on-resonance p-polarized light. (d) The angle-integrated EDCs for data in panels (a)–(c) f band peak positions are highlighted. The labels follow the common notation in Refs. [32–34]. The momentum cut taken with 121 eV photons crosses (0,0,7.08 $2\pi/c$), close to Γ, and is thus labeled as Γ-M for simplicity.

states is further corroborated by observing the hybridization with the bulk conduction bands (discussed below).

Figures 3(a) and 3(b) show the photoemission intensities taken off-resonance with 114-eV photons and on-resonance with 121-eV photons at 11 K, respectively, using s-polarized light. Here, the polarization is perpendicular to the plane defined by the incident light and emitted electrons, whereas the polarization of the p-polarized light is in the plane. Co $3d$ and Ce $5d$ states dominate the off-resonance spectra, and they are consistent with the data in Fig. 1 taken with soft x-rays. The Ce $4f$ state is strongly enhanced in the on-resonance data, as also shown by the integrated spectra in Fig. 3(d). Two nearly flat features can be observed in the on-resonance data, corresponding to the $4f^1_{5/2}$ and $4f^1_{7/2}$ states [32,33]. The feature near E_F is actually the tail of the Kondo resonance peak above E_F. Figure 3(c) shows the data taken with p-polarized light, where the f electron intensity is weaker than that taken with s-polarized light.

IV. TEMPERATURE DEPENDENCE OF THE f ELECTRONS

Figures 4(a)–4(c) display the evolution of the Fermi surface mapping of $CeCoIn_5$ measured at the resonant condition in

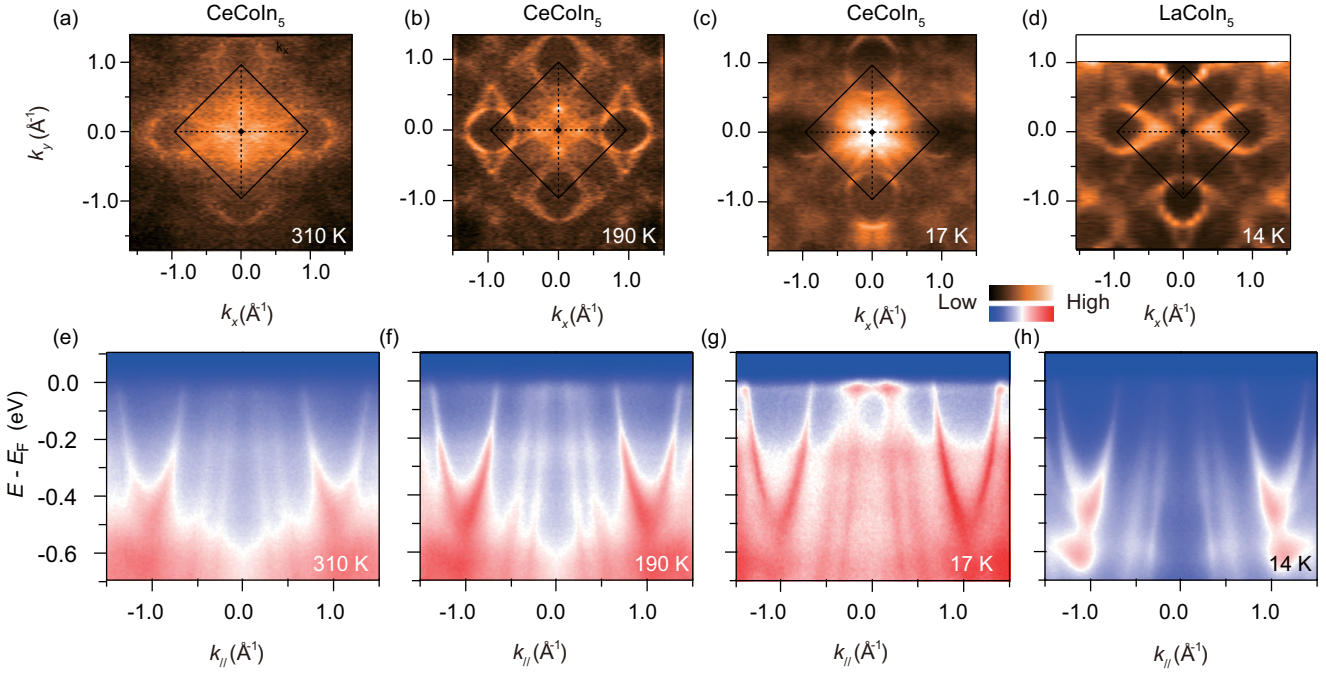

FIG. 4. f-d hybridization in $CeCoIn_5$ upon cooling. (a-c) Photoemission intensity maps of $CeCoIn_5$ taken at 310, 190, and 17 K, respectively. (d) Photoemission intensity map of $LaCoIn_5$ taken at 14 K. (e)–(g) Photoemission intensity distributions of $CeCoIn_5$ along Γ-M taken at 310, 190, and 17 K, respectively. (h) Photoemission intensity distribution of $LaCoIn_5$ along Γ-M taken at 14 K. All the data were taken with 121 eV s-polarized light, and the integration energy window for (a)–(d) is ($E_F - 10$ meV, $E_F + 10$ meV).

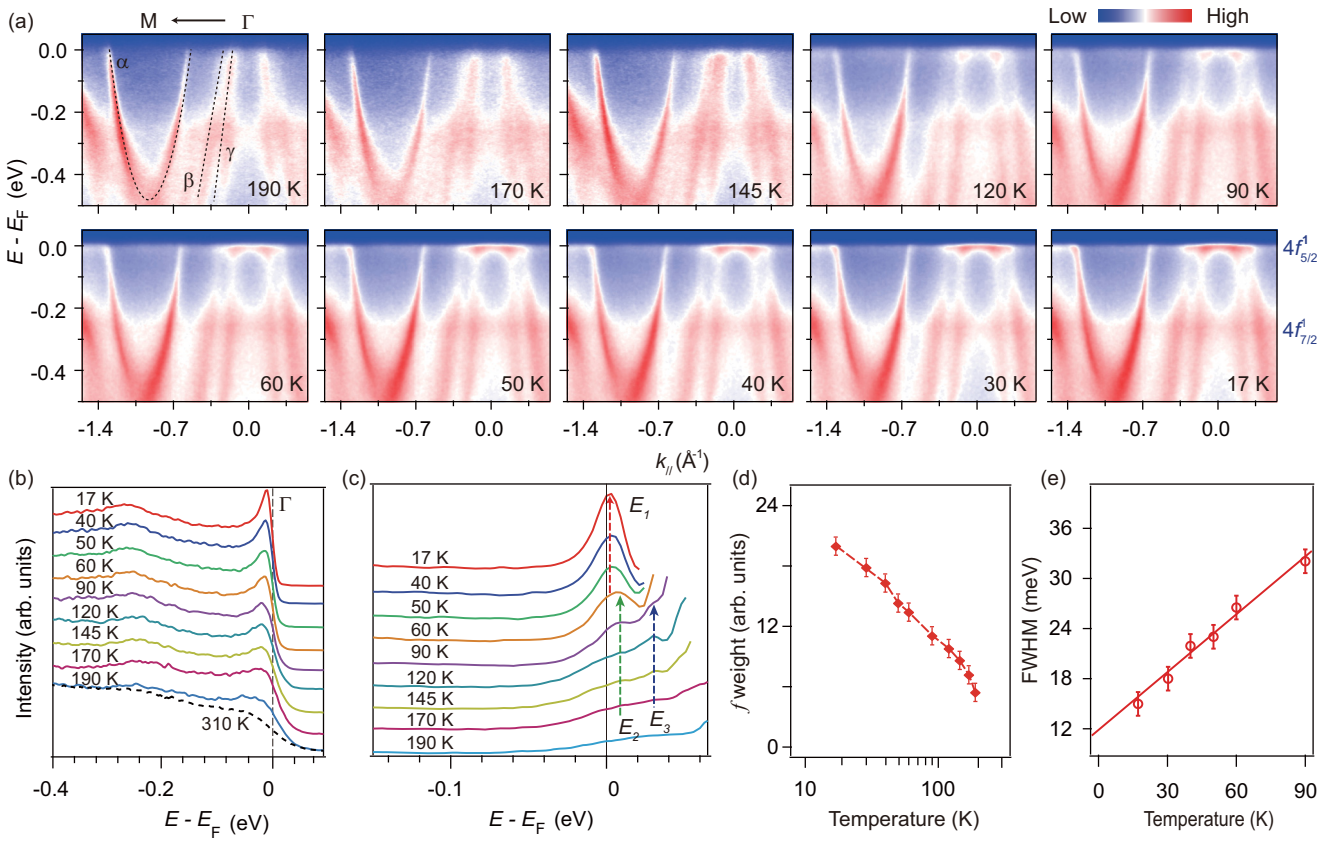

FIG. 5. Temperature evolution of the electronic structure of $CeCoIn_5$. (a) Resonant (121 eV) ARPES data of $CeCoIn_5$ along Γ-M at the labeled temperatures. The momentum cut taken with 121 eV photons crosses (0,0,7.08 $\frac{2\pi}{c}$), close to Γ, thus labeled hereafter as Γ-M for simplicity. (b) Temperature dependence of the EDCs at Γ. The dashed line denotes the result taken at 310 K from another sample (c) To reveal states above E_F, the spectra in (b) are divided by the RC-FDD at their respective temperatures. Three features at $E_1 = 2$ meV, $E_2 = 9$ meV, and $E_3 = 30$ meV can be observed. (d) The background-subtracted integrated quasiparticle spectral weight near E_F in the vicinity of Γ as a function of temperature on log-linear scale. This is calculated by integrating the left half of the main peak in panel (c) over [−40 meV, 2 meV] after subtracting the flat background over [−140 meV, −98 meV]. (e) Temperature dependence of the FWHM of the main Kondo resonance at E_1 in (c) below 90 K (circles), where the influences from the first excited CEF state and the finite energy resolution have been removed, following the analysis in Fig. S4 of Ref. [35]. The line is the best fit, giving FWHM [meV] $= 11.8 + 2.69 \times k_B T$ [K].

a large temperature range. At 310 K, the Fermi surface of $CeCoIn_5$ is essentially identical to that of $LaCoIn_5$ [Fig. 4(d)]. Their band structures shown in Figs. 4(e) and 4(h) are essentially identical as well, which both exhibit linear dispersion with large slopes near E_F. Because $LaCoIn_5$ lacks f electrons, this indicates that the f electrons in $CeCoIn_5$ are basically fully localized at 310 K. Upon decreasing temperature, the f spectral weight around Γ is gradually enhanced, and becomes pronounced at 17 K. In Figs. 4(f) and 4(g), the flat f band emerges near E_F and its hybridization with the conduction bands becomes more obvious, indicating that the f electrons become more itinerant. The contribution of f electrons to the Fermi surface can also be demonstrated by comparing the data taken "on" and "off" Ce $4d$-$4f$ resonance at low temperature. In Fig. S1 of Ref. [35], we present the data taken at off-resonance (85 eV), compared with the Fermi surface taken on-resonance (121 eV), the f spectral weight can be further confirmed. Such a behavior will be further discussed in the rest of this section.

Figure 5 shows a more detailed T evolution of the resonant ARPES data along Γ-M from 17 K to 190 K. At high T, the photoemission intensity is dominated by the strongly dispersive d bands. Upon decreasing temperature, two weakly dispersive f-electron features near E_F and −280 meV gradually emerge. Their T dependence is reflected in the energy distribution curves (EDCs) at Γ shown in Fig. 5(b). The f-electron feature near −280 meV originates from spin-flip (Kondo) scattering of the $4f_{7/2}$ states. Its overall T dependence thus resembles that of the quasiparticle peak near E_F. Differences arise from the higher degeneracy [split by crystal electric field (CEF) effects] and details of the hybridization matrix. A similar Kondo satellite peak is expected to appear at around 280 meV, i.e., above E_F [36]. To access features above E_F, the spectra are divided by the resolution-convoluted Fermi-Dirac distribution (RC-FDD) at corresponding temperatures and shown in Fig. 5(c). This allows us to identify three features located at 2, 9, and 30 meV above E_F, labeled as E_1, E_2, and E_3, respectively. The E_1 peak spectral weight gradually increases with decreasing T from 190 to 17 K [Fig. 5(d) and caption].

For $CeCoIn_5$, one expects the sixfold degenerate $4f_{5/2}$ state to be split into three Kramer's doublets by the tetragonal CEF. Each excited CEF doublet can participate in Kondo

scattering processes and give rise to Kondo resonance satellite peaks shifted from the main Kondo resonance [36]. The peak separations, $E_2 - E_1 \sim 7$ meV and $E_3 - E_1 \sim 28$ meV, are in excellent agreement with the CEF splittings estimated by neutron scattering [37]. Therefore we conclude that the features found here are crystal-field-split $4f_{5/2}$ states, with the main Kondo resonance peak at E_1 above E_F, as expected for a Ce-based heavy-fermion system [38]. Consistently, the temperature dependencies of the peak intensities also reflect temperature dependencies the populations of the CEF states, as shown in Fig. 8(b) later. Moreover, we find that $4f^1_{5/2}$ state is quite sensitive to the polarization of the light—a significant enhancement is seen under s-polarized light compared with p polarization [Fig. 3(c)]. Figure S2 enlarges the EDCs near E_F after dividing by the RC-FDD under different polarizations, from which a peak separation of ~6.5 meV can be found between the main Kondo resonance peak and the first excited satellite peak. The polarization dependence arises from the differences in the wave-function symmetry associated with different $4f^1_{5/2}$ states, which also confirms the bulk origin of the observed electronic structure (details can be found in Ref. [35] "on-resonance EDCs of $CeCoIn_5$ under different polarizations"). CEF splittings of the $4f^1_{7/2}$ Kondo satellite peak have not been resolved due to their intrinsic widths. Similar to the $4f^1_{7/2}$ peak, Kondo satellite peaks related to excited $4f^1_{5/2}$ (CEF) states can also appear below E_F but are typically much weaker and are hard to resolve [36,39]. These satellite peaks have, however, been observed in the antiferromagnet $CeRh_2Si_2$, where the reduced hybridization and concomitantly lower Kondo scales allow for the observation of CEF-derived Kondo satellites of the $4f^1_{5/2}$ states below E_F [32].

Our results demonstrate that the heavy band formation begins at much higher T than the previously conceived $T_{\rm coh}$, as can be inferred from, e.g., Fig. 5(a). A dispersive feature near E_F is already clearly discernible around 120 K. Figure 5(d) shows that the f-electron weight increases upon cooling from the highest measured T (190 K). Based on the extrapolation outlined in Fig. S3 of Ref. [35], we infer an onset at around 270 ± 30 K. This confirms the finding of a well-developed hybridization gap reported by a recent STM study at its highest T of 68 K [15].

It is commonly accepted that the CEF splittings can enhance the T_K when the CEF level separations and Kondo energy scale are comparable [36,40]. While it has been difficult to unambiguously identify CEF excitations in thermodynamic and transport measurements, particularly for $CeCoIn_5$, our observation of Kondo satellite peaks [Fig. 5(c)] supports the analysis of the CEF excitations of Bauer *et al.* [37], and suggest that the CEF excitations contribute to the observed high onset T of the Fermi surface increase in $CeCoIn_5$.

Figure 5(e) plots the single-particle scattering rate of the main Kondo resonance, represented by the full width at half maximum (FWHM) of the peak at E_1 in Fig. 5(c). Intriguingly, it shows a linear T dependence for $T \leqslant 90$ K, and the $T = 0$ width is extrapolated to be about 12 meV, which is compatible with the onset T of heavy band formation. Such a T-linear scattering rate has been observed in many unconventional superconductors [41–43], most notably the optimally-doped cuprates [44].

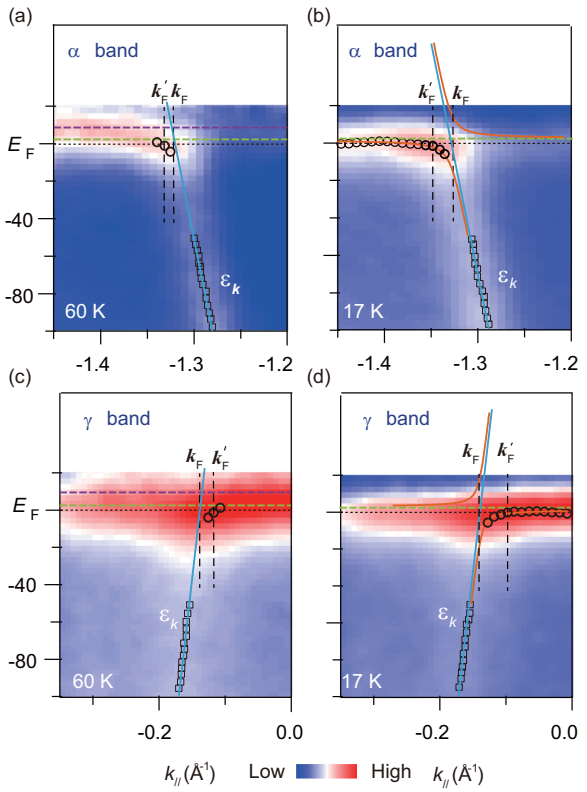

FIG. 6. Development of heavy electron states upon cooling. (a) and (b) Photoemission intensity distribution near the Fermi crossing of the α band taken at (a) 60 and (b) 17 K after divided by the RC-FDD. (c) and (d) same as (a) and (b) except they are near the Fermi crossing of the γ band. Circles represent the position of the hybridized f band obtained by tracking EDCs, squares represent the position of the conduction band at high temperature from fitting MDCs. The f-d hybridizations in (b) and (d) are modeled by the periodic Anderson model [Eq. (1), orange curves], where the blue lines denote the high-temperature band dispersions. E_1 and E_2 are indicated by dashed lines.

Figures 6(a) and 6(b) zoom into the vicinity of the Fermi crossing of α at 60 and 17 K, respectively, where the data have been divided by the corresponding RC-FDDs. Because of the influence of the first excited CEF state, the dispersion above E_F cannot be precisely traced in the 60 K data, however, one can clearly observe the Fermi velocity of α decreasing when going from 60 to 17 K. Compared to the high-T dispersion in Fig. 5(a) (see also Fig. S5 of Ref. [35]), the Fermi velocity of α is reduced by a factor of 24 ± 3 at 17 K. The γ band behaves similarly, as shown in Figs. 6(c) and 6(d). We note that due to the overlap of several bands, the hybridization of β cannot be resolved, but it is expected to behave similarly to α.

Phenomenologically, our 17-K data can be well described by a simple mean-field hybridization band picture based on the periodic Anderson model (PAM) [45] as presented in Figs. 6(b) and 6(d), in which the energy dispersion is given by

$$E^{\pm} = \frac{\varepsilon_0 + \varepsilon(k) \pm \sqrt{(\varepsilon_0 - \varepsilon(k))^2 + 4|V_k|^2}}{2}, \qquad (1)$$

where ε_0 is the renormalized f-level energy (the CEF ground state here), ε_k is the conduction-band dispersion at high tem-

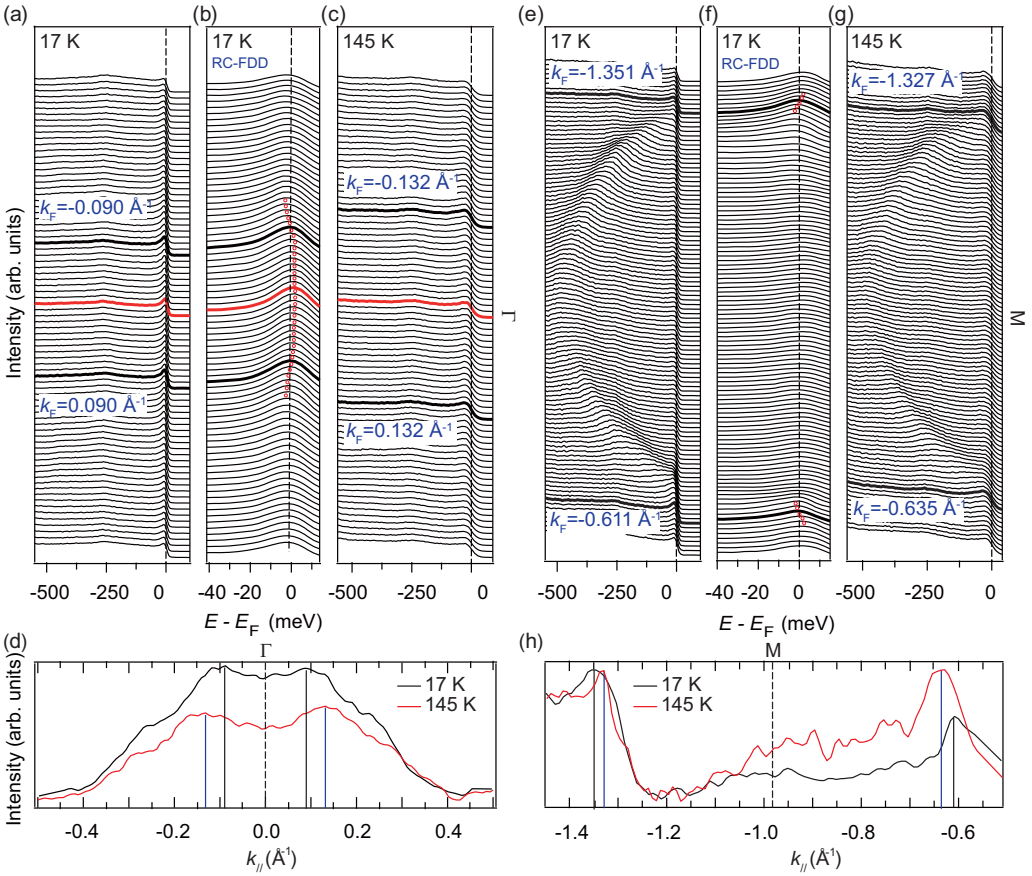

FIG. 7. Quantitative analysis of the enlargement of the α and γ band. (a) EDCs of the holelike γ band around Γ taken at 17 K. (b) EDCs of (a) divided by the RC-FDD in a smaller energy window to highlight the fine structure near E_F. The red circles mark the dispersion of the weakly dispersive hybridized band. A Fermi momentum (k_F) is determined based on the EDC whose peak is centered at E_F. The thick black curves denote the EDCs at k_F. The thick red curves denote the EDCs at the Γ point. (c) EDCs of the γ band in the same momentum region as (a), taken at 145 K. (d) The MDCs at E_F around Γ, taken at 17 and 145 K. (e) EDCs of the electronlike α band around M taken at 17 K. (f) EDCs of (e) divided by the RC-FDD in a smaller energy window to highlight the fine structures near E_F. (g) EDCs of the α band in the same momentum region as (e), taken at 145 K. (h) The MDCs at E_F around the M point, taken at 17 and 145 K.

peratures (Fig. S5), and V_k is the renormalized hybridization [34,45]. This is surprising, as the system is not in a Fermi liquid state, in contrast to the assumption underlying Eq. (1), nor does Eq. (1) capture any of the effects related to CEF excitations. A fit to this model gives $\varepsilon_0 = 2$ meV and $V_k = 15 \pm 5$ meV for both α and γ, respectively, corresponding to a direct gap (defined as the minimal separation of two bands at the same momentum) of 30 meV. The indirect gap is of the order of V_k^2/D, where D is of the order of the bandwidth of the α and γ band, respectively, and thus vanishingly small. The previous picture of a sizable indirect gap proposed by the STM study (and the hybridization model therein) thus appears to be an overestimate. Because the tunneling matrix element for the conduction band is much larger than that of the f electrons [15], STM mainly measures the direct gap, like optical conductivity [20].

In either Figs. 6(a) and 6(b) (for α) or Figs. 6(c) and 6(d) (for γ), the Fermi energy crossing (k'_F) departs from the high temperature position (k_F) as the temperature is lowered from 60 to 17 K, reflecting the transfer of spectral weight and the concomitant gradual inclusion of additional f electrons into the Fermi sea upon cooling into the heavy electron state. The Fermi surface expands in the heavy electron state, due to the inclusion of additional f electrons into the Fermi sea. Figure 7 presents a detailed quantitative analysis of the electron pocket around M and the hole pocket around Γ. Figures 7(a) and 7(b) plot the EDCs of the γ band taken at 17 K along Γ-M and the corresponding EDCs after dividing by the RC-FDD, respectively. The dispersion of the hybridized band is clearly visible in Fig. 7(b), and the Fermi momentum at low temperature can be determined when the peak passes E_F, which is labeled by the thick black lines. Alternatively, the same Fermi momenta could be obtained through the MDC maxima [Fig. 7(d)]. At high temperature, the k_Fs could be determined from the MDC maxima. Based on the quantitative analysis presented in Fig. 7, we estimate that the radius of the α electron pocket *expands* by 0.024 ± 0.008 Å^{-1} between 145 and 17 K, while the radius of the γ hole pocket *shrinks* by 0.042 ± 0.008 Å^{-1} in this temperature range. Considering the rather two-dimensional character of α and assuming an isotropic expansion, we estimate that 0.058 electrons have been transferred from the local f moment to the α pocket at low temperature. Similarly, we estimate that 0.032 holes are removed from the central γ pocket. Since the Fermi surfaces

in Figs. 4(a) and 4(c) do not show any other pronounced difference, by assuming the similar expansion of the β Fermi surface, we loosely estimate the upper limit of the total Fermi volume expansion to be about 0.2 ± 0.05 electrons in the localized-to-itinerant transition. The Kondo-screened ground state is expected to posses an enlarged Fermi volume due to the Kondo effect. Since the valency of Cerium is close to +3 and only weakly temperature-dependent, the size of the volume increase over the high-temperature Fermi volume of $CeCoIn_5$ is expected to equal one electron due to Luttinger's sum rule. In this sense, the $4f$ electrons on Cerium ions could be considered as fully itinerant. However, our data indicate that this Fermi volume increase is much smaller, i.e., the f electrons become only partially itinerant above 17 K, in contrast to various theories and calculations suggesting fully itinerant f electrons at such moderately low temperatures and the dramatic change of Fermi surface topology [7]. We expand on this point in Ref. [35].

V. INTERMITTENT E/T SCALING AND CEF EXCITATIONS

A recent STM study on $CeCoIn_5$ reported quantum critical E/T scaling of the local conductance to set in below 60 K and inferred a linear-in-T relaxation rate of the single-particle excitations [15]. Such E/T scaling reflects the scale-invariant quantum critical spectrum and the absence of any intrinsic energy scale other than T that pertains in the vicinity of interacting quantum critical points. While such E/T scaling has been reported for a number of heavy-fermion compounds close to a quantum critical point [46–48], its observation in $CeCoIn_5$ and its onset at elevated T seems surprising and incompatible with, e.g., the T evolution of the Seebeck coefficient [29].

Interestingly, our ARPES data also obey an E/T scaling between 90 and 30 K [Fig. 8(a)] in the vicinity of the Fermi energy with a fractional exponent ≈0.36 [49]. Notably, the 17- and 120-K data fail to show scaling. This implies that this approximate E/T scaling is an intermittent property and *not* directly related to quantum criticality. The absence of E/T scaling below roughly 20 K indicates that it does not underlie the linear-in-T behavior of the scattering rate that sets in around 20 K and persists down to the onset of superconductivity. In order to trace the possible origin of this anomalous T-dependent scaling, we show in Fig. 8(b) the anticipated occupation of the CEF-split $4f^1_{5/2}$ state, based on the obtained CEF splittings of 7 and 28 meV (see also Ref. [35]): below 20 K, essentially all $4f^1_{5/2}$ electrons occupy the lowest CEF doublet; above 20 K, the occupation of the first excited state increases with temperature, undergoing a smooth slope change around 90 K and leveling off slowly at higher T. This in turn indicates that the apparent scaling may be related to the depopulation of the excited CEF levels in $CeCoIn_5$ together with the various marked changes below 20 K, including the slope change of the Seebeck coefficient at 20 K, which commonly signals lattice coherent Kondo scattering, and the strong T and field dependence of the Nernst coefficient below 20 K [29]. In addition, the smooth onset of observed approximate E/T scaling as T is lowered coincides with the smooth increase in the depopulation rate

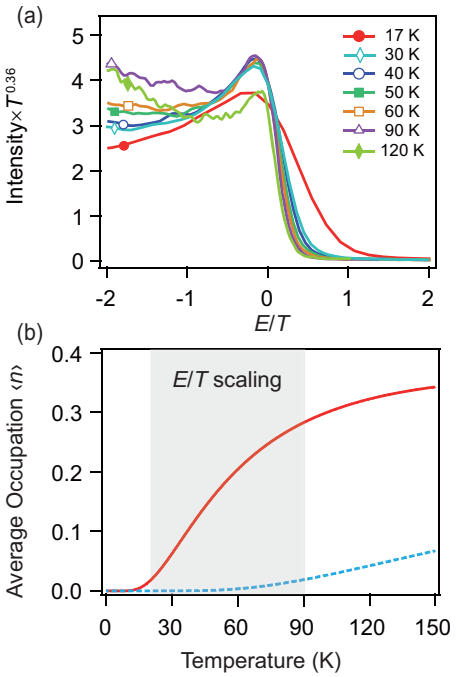

FIG. 8. Approximate E/T scaling and the CEF excitation occupations. (a) The EDCs at Γ are scaled by $T^{0.36}$ and plotted over E/T for individual temperatures. In this way, the E/T scaling can be fulfilled for data taken between 90 and 30 K. (b) Estimate of the average occupation of the first (red solid line) and second (blue dashed line) excited CEF doublets as a function of temperature assuming CEF splittings of 7 and 28 meV, see Ref. [35] for details. The gray region denotes the temperature range with E/T scaling.

of the excited levels as T drops below the lowest CEF gap at around 90 K. It would be interesting to see if this conjecture can be borne out by microscopic calculations and if the behavior of the single-particle spectrum between 20–90 K can also be observed in other correlation functions.

Understanding the emergence of unconventional superconductivity and quantum criticality in heavy fermions is linked to an understanding of the low-energy scales in these systems [50]. Our results strongly suggest that CEF effects play an unexpectedly significant role in the localized-to-itinerant transition of $CeCoIn_5$. The scope and significance of their involvement in the formation of the heavy-fermion state have so far not been fully appreciated. They will not only enhance T_K but also introduce additional characteristic temperatures, and may be ubiquitous to all the Ce-based rare-earth intermetallics.

Our results complement the existing experimental picture of the localized-to-itinerant transition in prototypical periodic Kondo lattice systems. Besides providing the first 3D Fermi surface mapping and experimental band structure of the heavy-fermion compound $CeCoIn_5$, we show how the localized f electrons become partially itinerant and evolve into the heavy-fermion state from much higher temperatures than $T_{coh} \approx 50$ K, and how the Fermi volume increases along the way. The observed T dependence of the electronic structure unambiguously indicates the importance of CEF excitations. Thus our results provide a nearly complete microscopic picture

of how the heavy fermions in $CeCoIn_5$ develop and evolve with T. This should prove helpful in obtaining a complete microscopic understanding of the emergence of unconventional superconductivity and quantum phase transitions in this and related compounds.

ACKNOWLEDGMENTS

We gratefully acknowledge enlightening discussions with Y. F. Yang and the experimental support of M. Hoesch, T. Kim, and X. P. Shen. This work is supported in part by the National Science Foundation of China (Grants No. 11504342 and No. U1630248); the Science and Technology Commission of Shanghai Municipality (Grant No. 15ZR1402900), National Key R&D Program of the MOST of China (Grant No. 2016YFA0300200), Science Challenge Project (No. TZ2016004), Center for Integrated Nanotechologies, a U.S. DOE Office of Basic Energy Sciences user facility, and Diamond Light Source for time on beamline I05 under Proposal No. SI11914. Soft x-ray ARPES was performed at the SX-ARPES endstation of the ADRESS beamline at the Swiss Light Source, Paul Scherrer Institute, Switzerland. F.B. is supported by the Swiss National Science Foundation (Grant No. 200021 146890) and European Community's Programme FP7/2007-2013 (Grant No. 290605 PSI-FELLOW/COFUND). Some preliminary data were taken at the ARPES beamline of the National Synchrotron Radiation Laboratory (NSRL).

[1] R. A. Copper, Y. Wang, B. Vignolle, O. J. Lipcombe, S. M. Hayden, Y. Tanabe, T. Adachi, Y. Koike, M. Bohara, H. Takagi, C. Proust, and N. E. Hussey, Anomalous criticality in the electrical resistivity of $La_{2-x}Sr_xCuO_4$, Science **323**, 603 (2009).

[2] S. Badoux, W. Tabis, F. Laliberté, G. Grissonnanche, B. Vignolle, D. Vignolles, J. Béard, D. A. Bonn, W. N. Hardy, R. Liang, N. Doiron-Leyraud, L. Taillefer, and C. Proust, Change of carrier density at the pseudogap critical point of a cuprate superconductor, Nature (London) **531**, 210 (2016).

[3] P. Coleman and A. H. Nevidomskyy, Frustration and the Kondo effect in heavy fermion materials, J. Low Temp. Phys. **161**, 182 (2010).

[4] C. M. Varma, Mixed-valence compounds, Rev. Mod. Phys. **48**, 219 (1976).

[5] G. R. Stewart, Heavy-fermion systems, Rev. Mod. Phys. **56**, 755 (1984).

[6] J. H. Shim, K. Haule, and G. Kotliar, Modeling the localized-to-itinerant electronic transition in heavy fermion system $CeIrIn_5$, Science **7318**, 1615 (2007).

[7] H. C. Choi, B. I. Min, J. H. Shim, K. Haule, and G. Kotliar, Temperature-Dependent Fermi Surface Evolution in Heavy Fermion $CeIrIn_5$, Phys. Rev. Lett. **108**, 016402 (2012).

[8] S.-K. Mo, W. S. Lee, F. Schmitt, Y. L. Chen, D. H. Lu, C. Capan, D. J. Kim, Z. Fisk, C.-Q. Zhang, Z. Hussain, and Z.-X. Shen, Emerging coherence with unified energy, temperature, and lifetime scale in heavy fermion $YbRh_2Si_2$, Phys. Rev. B **85**, 241103(R) (2012).

[9] K. Kummer, S. Patil, A. Chikina, M. Güttler, M. Höppner, A. Generalov, S. Danzenbächer, S. Seiro, A. Hannaske, C. Krellner, Yu. Kucherenko, M. Shi, M. Radovic, E. Rienks, G. Zwicknagl, K. Matho, J. W. Allen, C. Laubschat, C. Geibel, and D. V. Vyalikh, Temperature-independent Fermi surface in the Kondo lattice $YbRh_2Si_2$, Phys. Rev. X **5**, 011028 (2015).

[10] S.-I. Fujimori, Y. Saitoh, T. Okane, A. Fujimor, H. Yamagami, Y. Haga, E. Yamamoto, and Y. Ōnuki, Itinerant to localized transition of f electrons in the antiferromagnetic superconductior UPd_2Al_3, Nat. Phys. **3**, 618 (2007).

[11] Q. Si, S. Rabello, K. Ingersent, and J. Lleweilun Smith, Locally critical quantum phase transitions in strongly correlated metals, Nature (London) **413**, 804 (2001).

[12] S. Paschen, T. Lühmann, S. Wirth, P. Gegenwart, O. Trovarelli, C. Geibel, F. Steglich, P. Coleman, and Q. Si, Hall-effect evolution across a heavy-fermion quantum critical point, Nature (London) **432**, 881 (2004).

[13] C. M. Varma, Quantum-critical fluctuations in 2D metals: Strange metals and superconductivity in antiferromagnets and in cuprates, Rep. Prog. Phys. **79**, 082501 (2016).

[14] S.-I. Fujimori, Band structures of 4f and 5f materials studied by angle-resolved photoelectron spectroscopy, J. Phys.: Condens. Matter **28**, 153002 (2016).

[15] P. Aynajian, E. H. da Silva Neto, A. Gyenis, R. E. Baumbach, J. D. Thompson, Z. Fisk, E. D. Bauer, and A. Yazdani, Visualizing heavy fermions emerging in a quantum critical Kondo lattice, Nature (London) **486**, 201 (2012).

[16] S. Ernst, S. Kirchner, C. Krellner, C. Geibel, G. Zwicknagl, F. Steglich, and S. Wirth, Emerging local Kondo screening and spatial coherence in the heavy-fermion metal $YbRh_2Si_2$, Nature (London) **474**, 362 (2011).

[17] S. Paschen, S. Friedemann, S. Wirth, F. Steglich, S. Kirchner, and Q. Si, Kondo destruction in heavy fermion quantum criticality and the photoemission spectrum of $YbRh_2Si_2$, J. Magn. Magn. Mater. **400**, 17 (2016).

[18] H. Shishido, R. Settai, D. Aoki, S. Ikeda, H. Nakawaki, N. Nakamura, T. Iizuka, Y. Inada, K. Sugiyama, T. Takeuchi, K. Kindo, T. C. Kobayashi, Y. Haga, H. Harima, Y. Aoki, T. Namiki, H. Sato, and Y. Ōnuki, Fermi surface, magnetic and superconducting properties of $LaRhIn_5$ and $CeTIn_5$ (T: Co, Rh and Ir), J. Phys. Soc. Jpn. **71**, 162 (2002).

[19] R. Settai, H. Shishido, S. Ikeda, Y. Murakawa, M. Nakashima, D. Aoki, Y. Haga, H. Harima, and Y. Ōnuki, Quasi-two-dimensional Fermi surfaces and the de Haas-van Alphen oscillation in both the normal and superconducting mixed states of $CeCoIn_5$, J. Phys.: Condens. Matter **13**, L627 (2001).

[20] E. J. Singley, D. N. Basov, E. D. Bauer, and M. B. Maple, Optical conductivity of the heavy fermion superconductor $CeCoIn_5$, Phys. Rev. B **65**, 161101(R) (2002).

[21] K. S. Burch, S. V. Dordevic, F. P. Mena, A. B. Kuzmenko, D. van der Marel, J. L. Sarrao, J. R. Jeffries, E. D. Bauer, M. B. Maple, and D. N. Basov, Optical signatures of momentum-dependent hybridization of the local moments and conduction electrons in Kondo lattices, Phys. Rev. B **75**, 054523 (2007).

[22] M. P. Allan, F. Massee, D. K. Morr, J. Van Dyke, A. W. Rost, A. P. Mackenzie, C. Petrovic, and J. C. Davis, Imaging Cooper pairing of heavy fermions in $CeCoIn_5$, Nat. Phys. **9**, 468 (2013).

[23] B. B. Zhou, S. Misra, E. H. da Silva Neto, P. Aynajian, R. E. Baumbach, J. D. Thompson, E. D. Bauer, and A. Yazdani,

Visualizing nodal heavy fermion superconductivity in $CeCoIn_5$, Nat. Phys. **9**, 474 (2013).

[24] K. Haule, C.-H. Yee, and K. Kim, Dynamical mean-field theory within the full-potential methods: Electronic structure of $CeIrIn_5$, $CeCoIn_5$, and $CeRhIn_5$, Phys. Rev. B **81**, 195107 (2010).

[25] A. Koitzsch, T. K. Kim, U. Treske, M. Knupfer, B. Büchner, M. Richter, I. Opahle, R. Follath, E. D. Bauer, and J. L. Sarrao, Band-dependent emergence of heavy quasiparticles in $CeCoIn_5$, Phys. Rev. B **88**, 035124 (2013).

[26] A. Koitzsch, S. V. Borisenko, D. Inosov, J. Geck, V. B. Zabolotnyy, H. Shiozawa, M. Knupfer, J. Fink, B. Büchner, E. D. Bauer, J. L. Sarrao, and R. Follath, Hybridization effects in $CeCoIn_5$ observed by angle-resolved photoemission, Phys. Rev. B **77**, 155128 (2008).

[27] A. Koitzsch, I. Opahle, S. Elgazzar, S. V. Borisenko, J. Geck, V. B. Zabolotnyy, D. Inosov, H. Shiozawa, M. Richter, M. Knupfer, J. Fink, B. Büchner, E. D. Bauer, J. L. Sarrao, and R. Follath, Electronic structure of $CeCoIn_5$ from angle-resolved photoemission spectroscopy, Phys. Rev. B **79**, 075104 (2009).

[28] C. Petrovic, P. G. Pagliuso, M. F. Hundley, R. Movshovich, J. L. Sarrao, J. D. Thompson, Z. Fisk, and P. Monthoux, Heavy-fermion superconductivity in $CeCoIn_5$ at 2.3 K, J. Phys.: Condens. Matter **13**, L337 (2001).

[29] R. Bel, K. Behnia, Y. Nakajima, K. Izawa, Y. Matsuda, H. Shishido, R. Settai, and Y. Onuki, Giant Nernst in $CeCoIn_5$, Phys. Rev. Lett. **92**, 217002 (2004).

[30] V. N. Strocov, M. Shi, M. Kobayashi, C. Monney, X. Wang, J. Krempasky, T. Schmitt, L. Patthey, H. Berger, and P. Blaha, Three-Dimensional Electron Realm in VSe_2 by Soft-X-Ray Photoemission Spectroscopy: Origin of Charge-Density Waves, Phys. Rev. Lett. **109**, 086401 (2012).

[31] C. Pfleiderer, Superconducting phases of f-electron compounds, Rev. Mod. Phys. **81**, 1551 (2009).

[32] S. Patil, A. Generalov, M. Güttler, P. Kushwaha, A. Chikina, K. Kummer, T. C. Rödel, A. F. Santander-Syro, N. Caroca-Canales, C. Geibel, S. Danzenbächer, Y. Kucherenko, C. Laubschat, J. W. Allen, and D. V. Vyalikh, ARPES view on surface and bulk hybridization phenomena in the antiferromagnetic Kondo lattice $CeRh_2Si_2$, Nat. Commun. **7**, 11029 (2016).

[33] S.-i Fujimori, A. Fujimori, K. Shimada, T. Narimura, K. Kobayashi, H. Namatame, M. Taniguchi, H. Harima, H. Shishido, S. Ikeda, D. Aoki, Y. Tokiwa, Y. Haga, and Y. Ōnuki, Direct observation of a quasiparticle band in $CeIrIn_5$: An angle-resolved photoemission spectroscopy study, Phys. Rev. B **73**, 224517 (2006).

[34] H. J. Im, T. Ito, H.-D. Kim, S. Kimura, K. E. Lee, J. B. Hong, Y. S. Kwon, A. Yasui, and H. Yamagami, Direct Observation of Dispersive Kondo Resonance Peaks in a Heavy-Fermion System, Phys. Rev. Lett. **100**, 176402 (2008).

[35] See Supplemental Material at http://link.aps.org/supplemental/10.1103/PhysRevB.96.045107 for direct observation of how the heavy-fermion state develops in $CeCoIn_5$.

[36] J. Kroha, S. Kirchner, G. Sellier, P. Wölfle, D. Ehm, F. Reiner, S. Hüfner, and C. Geibel, Structure and transport in multi-orbital Kondo systems, Physica E **18**, 69 (2003).

[37] E. D. Bauer, A. D. Christianson, J. M. Lawrence, E. A. Goremychkin, N. O. Moreno, N. J. Curro, F. R. Trouw, J. L. Sarrao, J. D. Thompson, R. J. McQueeney, W. Bao, and R. Osborn, Crystalline electric field excitations in the heavy fermion superconductor $CeCoIn_5$, J. Appl. Phys. **95**, 7201 (2004).

[38] We note that the heights of the satellite CEF peaks appear stronger than that of the main one at high temperatures, which may be due to matrix element effects or a divergence artifact from the division by RC-FDD high above E_F.

[39] D. Ehm, S. Hüfner, F. Reinert, J. Kroha, P. Wölfle, O. Stockert, C. Geibel, and H. v. Löhneysen, High-resolution photoemission study on low-T_K Ce systems: Kondo resonance, crystal field structures, and their temperature dependence, Phys. Rev. B **76**, 045117 (2007).

[40] B. Cornut, and B. Coqblin, Influence of the crystalline field on the Kondo effect of alloys and compounds with cerium impurities, Phys. Rev. B **5**, 4541 (1972).

[41] R. Daou, N. Doiron-Leyraud, D. LeBoeuf, S. Y. Li, Francis. Laliberté, O. Cyr-Choinière, Y. J. Jo, L. Balicas, J. Q. Yan, J. S. Zhou, J. B. Goodenough, and L. Taillefer, Linear temperature dependence of resistivity and charge in the Fermi surface at the pseudogap critical point of a high-T_c superconductor, Nat. Phys. **5**, 31 (2009).

[42] Y. M. Dai, B. Xu, B. Shen, H. Xiao, H. H. Wen, X. G. Qiu, C. C. Homes, and R. P. S. M. Lobo, Hidden T-Linear Scattering Rate in $Ba_{0.6}K_{0.4}Fe_2As_2$ Revealed by Optical Spectroscopy, Phys. Rev. Lett. **111**, 117001 (2013).

[43] J. A. N. Bruin, H. Sakai, R. S. Perry, and A. P. Mackenzie, Similarity of scattering rates in metals showing T-linear resistivity, Science **339**, 804 (2013).

[44] T. Valla, A. V. Fedorov, P. D. Johnson, B. O. Wells, S. L. Hulbert, Q. Li, G. D. Gu, and N. Koshizuka, Evidence of quantum critical behavior in the optimally doped cuprate $Bi_2Sr_2CaCu_2O$, Science **285**, 2110 (1999).

[45] A. C. Hewson, *The Kondo Problem to Heavy Fermions* (Cambridge University Press, Cambridge, 1993).

[46] M. C. Aronson, R. Osborn, R. A. Robinson, J. W. Lynn, R. Chau, C. L. Seaman, and M. B. Maple, Non-Fermi-Liquid Scaling of the Magnetic Response in $UCu_{5-x}Pd_x$ ($x = 1,1.5$), Phys. Rev. Lett. **75**, 725 (1995).

[47] A. Schröder, G. Aeppli, E. Bucher, R. Ramazashvili, and P. Coleman, Scaling of Magnetic Fluctuations Near a Quantum Phase Transition, Phys. Rev. Lett. **80**, 5623 (1998).

[48] S. Friedemann, N. Oeschler, S. Wirth, C. Krellner, C. Geibel, F. Steglich, S. Paschen, S. Kirchner, and Q. Si, Fermi-surface and dynamical scaling near a quantum-critical point, Proc. Natl. Acad. Sci. USA **107**, 14547 (2010).

[49] Such an E/T scaling could be observed at momenta where the f states dominate the spectra near E_F. To obtain the single-particle spectral function from the data shown in Fig. 3(b), the data need to be divided by the Fermi Dirac distribution function. This, however, is a function of E/T only and cannot spoil the scaling properties shown in Fig. 5(b).

[50] O. Stockert, S. Kirchner, F. Steglich, and Q. Si, Superconductivity in Ce- and U-based "122" heavy fermion compounds, J. Phys. Soc. Jpn. **81**, 011001 (2012).